Polymer Chemistry

ROYAL SOCIETY OF CHEMISTRY

PAPER

View Article Online
View Journal | View Issue

Cite this: *Polym. Chem.*, 2026, **17**, 1109

Real-time monitoring of photoinduced atom transfer radical polymerization by time-resolved diffusion NMR

Marek Czarnota, [a] Martyna Cybularczyk-Cecotka, [b] Franz F. Westermair, [c] Francisco Arrabal Campos, [d] Kriti Kapil, [e] Krzysztof Matyjaszewski, [e] Grzegorz Szczepaniak *[b] and Mateusz Urbańczyk *[a]

Conventional real-time monitoring of polymerization is a laborious process that requires offline sampling and analysis. In this work, we introduce an advanced approach that combines Time-Resolved Diffusion NMR with ^{1}H NMR for the simultaneous, *in situ* tracking of both monomer conversion and molecular weight evolution. We successfully applied this method to monitor the photoinduced atom transfer radical polymerization (photo-ATRP) in real-time. Furthermore, by coupling the gamma model with dispersity-matched accumulation, we accurately determined the dispersity values of the resulting polymers. To make the method more accessible, we developed a user-friendly program that sets up the acquisition and simplifies real-time monitoring of photo-ATRP. Additionally, the program allows stopping illumination at any desired monomer conversion, enabling easy control of the process.

Received 30th January 2026,
Accepted 18th February 2026

DOI: 10.1039/d6py00103c

rsc.li/polymers

Introduction

Synthetic polymers represent one of the most widely used classes of chemical compounds, enabling applications from everyday packaging to advanced drug delivery systems. The precise control over their properties, such as molecular weight, architecture, and functionality, is paramount. This necessity has driven the development of reversible-deactivation radical polymerization (RDRP) techniques,[1,2] with atom transfer radical polymerization (ATRP) standing out as a particularly powerful and versatile method since its discovery in 1995.[3,4]

However, conventional ATRP requires high concentrations of an air-sensitive copper(I) catalyst. To overcome this limitation, photoinduced ATRP (photo-ATRP) was developed,[5] which leverages light as a clean and efficient external stimulus to mediate the polymerization. This approach provides exceptional spatiotemporal control,[6] as the reaction can be initiated and halted simply by switching a light source on or off. Furthermore, photo-ATRP can be conducted in green solvents,[7] including water,[8] broadening the scope of compatible monomers and initiators.[9,10] It also exhibits greater tolerance to molecular oxygen,[11] eliminating the need for stringent deoxygenation procedures.

These features make photo-ATRP a highly promising method for both academic research and industrial manufacturing. However, its implementation and scalability are hindered by a critical challenge: photochemical reactions are extremely sensitive to subtle variations in experimental conditions.[12] Factors like light source intensity, reactor geometry, distance from the light source, and the homogeneity of the reaction mixture can profoundly impact polymerization kinetics and its reproducibility.[13] Minor, often unavoidable, deviations between experiments can lead to inconsistent outcomes, creating a significant barrier to the use of this technique.

This inherent sensitivity underscores a pressing need for robust analytical methods capable of monitoring the reaction's progress in real-time and under true process conditions (*in situ*).[14] Such tools are essential for understanding reaction kinetics, ensuring reproducibility, and enabling the effective optimization of polymerization conditions. The ongoing quest to develop tools for online polymerization monitoring has led to several key methods,[15] including electrospray ionization mass spectrometry,[16] *infra*-red spectroscopy,[17] chromatography,[18] and nuclear magnetic resonance (NMR).[19]

NMR monitoring has become one of the workhorses of modern chemists. However, this field is still growing in terms of methodology, showing progress from basic ^{1}H one-dimen-

[a]*Institute of Physical Chemistry, Polish Academy of Sciences, Kasprzaka 44/52, 01-224 Warszawa, Poland. E-mail: murbanczyk@ichf.edu.pl*
[b]*Faculty of Chemistry, University of Warsaw, Pasteura 1, 02-093 Warszawa, Poland. E-mail: g.szczepaniak@uw.edu.pl*
[c]*Faculty of Chemistry and Pharmacy, University of Regensburg, Universitätsstraße 31, 93053 Regensburg, Germany*
[d]*Department of Engineering, Research Centre CIAIMBITAL, University of Almería, 04120 Almería, Spain*
[e]*Department of Chemistry, Carnegie Mellon University, Pittsburgh, Pennsylvania 15213, USA*

sional series of spectra, *e.g.*, ref. 20 and 21 to different approaches like multidimensional spectroscopy for more complex systems.[22–28]

In the case of polymerization, researchers usually utilize ^{1}H NMR to monitor monomer conversion.[19,29,30] Additional approaches which can be used are ^{13}C MAS NMR,[31] or the Diffusion-NMR which is rapidly being utilized to monitor time-dependent processes.[27,28,32] This class of NMR is based on the analysis of the diffusion coefficient change in time instead of conventional frequency-based analysis. This approach allows a better insight into a process where the peak structure does not change (or changes insignificantly) while the molecular weight or freedom of movement is evolving. One of the most popular classes of reactions that fit the system above is polymerization. Usually, the molecular weight of the polymer changes significantly while the NMR spectrum of the polymer stays the same.

For such a system, diffusion NMR seems to be an ideal solution as the diffusion coefficient is linked to the molecular weight.[33] However, conventional diffusion NMR is not best suited for reaction monitoring. As the measurement time of a single experiment varies from minutes to hours, the temporal information can be lost. Additionally, the change in the concentration of reagents can affect the measured diffusion coefficients.[31]

Two acquisition strategies have been implemented to overcome this problem. The first, based on the spatial encoding of the diffusion coefficient, is called ultra-fast.[28,34,35] The second is based on the time-resolved non-uniform sampling,[36] where instead of randomly sampling the t_1 evolution time, one samples pulsed field gradients in the PGSTE sequence.[37,38] Both methods have strengths and weaknesses, and choosing the proper acquisition strategy is essential for the proper analysis.[39]

In this work, we utilized the Time-Resolved Diffusion NMR (TR-DNMR) as this method has proven successful for monitoring polymerization processes.[27,40] Additionally, the photo-ATRP process is light-driven; therefore, to study the process *in situ*, illumination must be provided to the NMR tube. The NMR community has proposed several approaches.[41–44] Currently, the most commonly used solution is to provide the illumination using an optical fiber with a polished tip that is inserted into the NMR tube.[45] This allows for uniform illumination of the sample volume and enables easy switching of the light source.

Results and discussion

In situ polymerization and light control

We employed a photo-ATRP method that combines organic photoredox catalysis with copper catalysis (Fig. 1).[30,46] A key advantage of this dual catalytic system is its high oxygen tolerance, which enables efficient polymerization under green light illumination without needing prior deoxygenation.[30] This approach yields well-defined polymers over a wide range of targeted degrees of polymerization (DP_T).[47–49]

To monitor the reaction in real-time, polymerizations were conducted inside an NMR tube illuminated by a centrally positioned optical fiber. A portion of the fiber was stripped from its cladding and polished. A New Era Photo-NMR device was used to ensure a stable fiber alignment, minimizing interference with magnetic field homogeneity. The polished end of the fiber was inserted in a way that the whole sample was

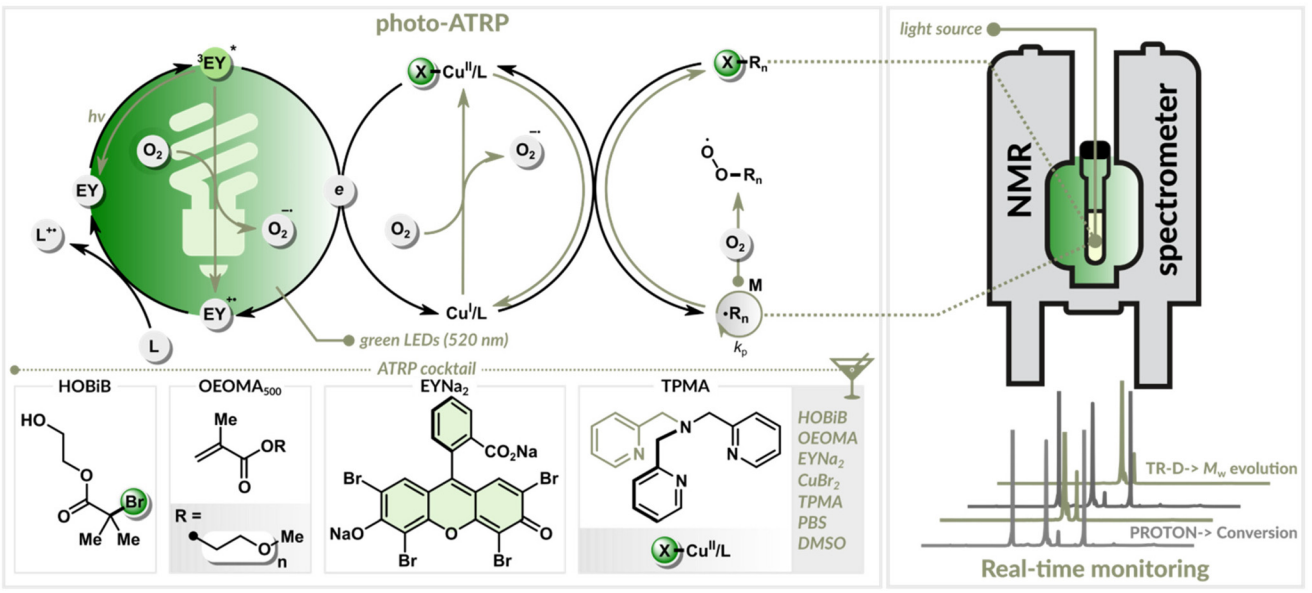

Fig. 1 Proposed mechanism for EY/Cu-catalyzed photo-ATRP and an illustration of the NMR setup used to monitor the polymerization. The setup combines *in situ* green light illumination with interleaved ^{1}H and TR-D experiments.

evenly illuminated. The LED illumination (520 nm) was controlled by an Arduino module, while a custom-written program with a graphical user interface (GUI) managed the experiment. This automated system provided real-time monitoring of monomer conversion, polymer diffusion coefficient, and molecular weight evolution. The system was programmed to automatically halt the polymerization by turning off the light once a predefined monomer conversion was achieved.

To demonstrate the effectiveness of this *in situ* monitoring technique, we performed a series of polymerizations (Table 1). The experiments used oligo(ethylene glycol) methyl ether methacrylate ($OEOMA_{500}$) as the benchmark water-soluble monomer. The other components were 2-hydroxyethyl 2-bromoisobutyrate (HOBiB) as the initiator, eosin Y disodium salt ($EYNa_2$) as the organic photoredox catalyst, and a $CuBr_2$/TPMA complex (TPMA = tris(2-pyridylmethyl)amine) as the copper catalyst. The polymerizations were conducted in phosphate-buffered saline (PBS 1X) containing 10% v/v non-deuterated dimethyl sulfoxide (DMSO). The targeted DP was varied by adjusting the HOBiB concentration (6.0–0.375 mM), while all other component concentrations remained fixed (Table 1).

The EY/Cu-catalyzed photo-ATRP process began with an induction period of approximately 200 min, during which dissolved oxygen was consumed (Fig. 2B). In this initial stage, oxygen quenched the excited photocatalyst and oxidized the copper(I) activator (Cu^I/L) (Fig. 1). Once the oxygen concentration dropped below a critical threshold, the polymerization started. The excited photocatalyst reduced the copper(II) deactivator (X–Cu^{II}/L), regenerating the Cu^I/L activator needed for polymer growth. Precise control was maintained through the reversible equilibrium between the activating Cu(I) and deactivating Cu(II) species, ensuring controlled, uniform growth of polymer chains (Fig. 1).[50]

Achieving precise control over monomer conversion is crucial for tailoring a polymer's final physical properties, such as its viscosity, glass transition temperature, and mechanical behavior. We demonstrated the versatility of our *in situ* NMR monitoring method by automatically stopping the light illumination once the desired monomer conversion was achieved. For reactions targeting a DP between 50 and 200, the process was stopped at 90% monomer conversion. For higher DP_T of 400 and 800, the reactions were halted at 70% conversion to diminish the dead-chain fraction (defined as the ratio of the concentration of terminated polymer chains to the initial concentration of the initiator).[51] As shown in Table 1, the resulting polymers exhibited low dispersity values and molecular weights ($M_{n,SEC}$) in close agreement with theoretical values ($M_{n,th}$), confirming the well-controlled nature of this technique.

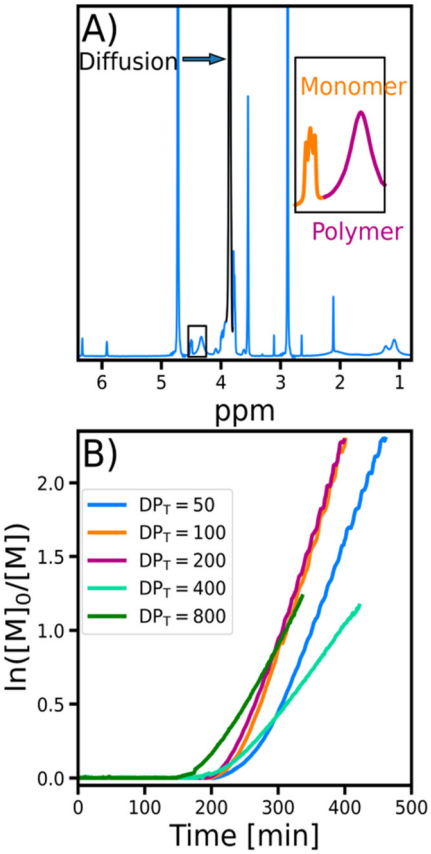

Fig. 2 The representative ^{1}H NMR spectrum taken during the polymerization (A). The inset provides a zoomed-in view that clearly distinguishes the peak of the unreacted monomer (orange, 4.55 ppm) from that of the newly formed polymer (magenta, 4.33 ppm). The peak at 3.85 ppm results from the overlap of monomer and polymer peaks and is used to monitor the diffusion coefficient. The polymerization kinetics at different DP_T (B).

Table 1 Photo-ATRP of $OEOMA_{500}$ with varying degrees of polymerization[a]

Entry	DP_T	Conv.[b]	$M_{n,th}$[c]	$M_{w,SEC}$	$M_{n,SEC}$	$Đ_{SEC}$	$Đ_{NMR}$[f]
1[d]	50	90%	22 700	26 400	21 900	1.20	1.17
2[d]	100	90%	45 200	56 000	45 300	1.24	1.25
3[d]	200	90%	90 200	96 300	84 500	1.14	1.08
4[e]	400	70%	140 200	158 700	139 100	1.11	1.12
5[e]	800	70%	280 200	374 900	251 100	1.39	1.37

[a] Reaction conditions [$OEOMA_{500}$] = 300 mM, [HOBiB] = 6.0–0.375 mM, [$EYNa_2$] = 15 μM, [$CuBr_2$] = 0.3 mM, [TPMA] = 0.9 mM in PBS with DMSO (10% v/v), irradiated under green LEDs (520 nm) in NMR tube. [b] Monomer conversion was determined by using ^{1}H NMR spectroscopy. [c] $M_{n,th}$ = DP_T × conv. × $MW_{OEOMA500}$ + MW_{HOBiB}. [d] Molecular weight ($M_{n,SEC}$ and $M_{w,SEC}$) and dispersity ($Đ_{SEC}$) were determined by size-exclusion chromatography (SEC) with a multi-angle light scattering (MALS) detector (DMF as eluent). [e] $M_{w,SEC}$, $M_{n,SEC}$ and $Đ_{SEC}$ were determined by Mark–Houwink calibration. [f] Dispersity ($Đ_{NMR}$) was determined by NMR diffusion measurements.

Time-resolved diffusion NMR

To monitor the evolution of molecular weight during the polymerization (Fig. 2), Time-Resolved Diffusion NMR (TR-DNMR) was used.[37,38] This method combines the diffusion NMR equivalent of the Time-Resolved Non-Uniform Sampling (TR-NUS)[36,52,53] and permuted Diffusion Ordered Spectroscopy (p-DOSY) concepts.[54]

The p-DOSY technique was introduced to eliminate the interference from the kinetics on the diffusion coefficient. The concept is simple: instead of sampling the pulsed field gradient strengths in ascending order, they are permuted. This makes the signal intensity change due to kinetics independent of the gradient strength. The TR-NUS technique was introduced to enable the monitoring of reactions with 2D NMR. In this approach, the evolution step of the indirect dimension is randomly sampled during the reaction. After the acquisition, the data are artificially separated into overlapping subsets, and the whole spectra are reconstructed.[55] Because the average time interval between these subsets is very short, the reconstructed data allow the reaction to be followed with high temporal resolution. We combined both concepts to monitor the evolution of the diffusion coefficient during the polymerization with excellent temporal resolution (the interval between points was 1 m 12 s).

In TR-DNMR, the concept is based on a series of PGSTE experiments, where the series of gradient strengths is permuted and repeated throughout the reaction time. Then, the data are divided into p-DOSY subsets, which are used to calculate the diffusion coefficients by fitting a mono-exponential model or an inverse Laplace transform.[56] Additionally, this approach allows the use of interleaved (IL) acquisition,[25] in which each step of the TR-DNMR experiment can be combined with a different one. In this work, we have interleaved the diffusion experiments with 1D proton experiments to calculate the monomer conversions.

The diffusion coefficients (D) were derived from TR-DNMR experiments. The experiments were divided into subsets of size 16, overlapping with each other by 15 experiments, so that each subset contained the same set of gradients. To determine the polymer diffusion coefficient (D_p), the peak at 3.85 ppm was integrated and its intensity ($I(b)$) was fitted with a double exponential model:

$$I(b) = I_0 C e^{-D_p \times b} + I_0(1 - C)e^{-D_m \times b} \quad (1)$$

where C is conversion, D_m is monomer diffusion coefficient, I_0 is signal intensity for gradient strength equal to zero, and

$$b = (\gamma G \delta)^2 \left(\Delta - \frac{\delta}{3}\right), \quad (2)$$

where γ is the magnetogyric ratio, G is the gradient strength, δ is the gradient pulse duration, and Δ is the time between gradient pulses. For additional numerical stability, the D_m value was fixed to 2.29×10^{-10} m^2 s^{-1}. This allowed us to follow the evolution of diffusion coefficients of the polymer as a function of time (Fig. 3A) and monomer conversion (Fig. 3B).

In the early stages of the polymerization (conv. <15%), the diffusion coefficient estimation had a significant fitting error due to the low intensity of the polymer signal compared to that of the monomer. However, after this initial disturbance, the evolution of the diffusion coefficient followed a similar path for all samples. The regular small fluctuations of the diffusion coefficients were caused by the repetitive sampling of pulsed field gradients. Additionally, we calculated the evolution of the weight-average molecular weight (M_w) from the diffusion coefficients using the equation:

$$D = kM_w{}^{\alpha}, \quad (3)$$

where k and α are scaling parameters obtained by fitting eqn (1) with diffusion data obtained during the polymerization and M_w acquired from size-exclusion chromatography (SEC) measurements. Except for the early stage of the process (conv. <15%), the molecular weight evolution follows an almost linear increase with time (Fig. 3C). It is worth mentioning that for systems where the viscosity changes during reaction, more advanced approaches than eqn (3) might be needed.[57–61]

Dispersity-matched accumulation diffusion NMR

NMR diffusion measurements can be used to calculate the polymer dispersity ($Đ$).[37,62,63] This method relies on modelling the non-monoexponential decay of the diffusion signal, for which a gamma distribution model can be used.[62] The data are fitted using a modified version of the conventional Stejskal-Tanner equation:[64]

$$I(b) = I_0(1 + b\sigma^2/D)^{(-D^2/\sigma^2)} \quad (4)$$

where σ is a standard deviation in the gamma distribution model of dispersity. As in this case, diffusion coefficients were different than those during polymerization due to temperature difference, new parameters k and α were calculated and used in dispersity estimation:

$$Đ = \left(1 + \frac{\sigma^2}{D^2}\right)^{\frac{1}{\alpha^2}} \quad (5)$$

However, as shown in Fig. 4, for samples with dispersity values below 2, the deviation from the classical mono-exponential model is visible only for high gradients, where the signal-to-noise ratio is significantly diminished. This causes difficulty in fitting the gamma model for experiments with a moderate number of scans and necessitates extremely long experiments with many transient acquisitions. Such an approach is far from optimal, especially for the points with low gradient strength, where the SNR is high, and multiple scans do not increase the data quality.

To overcome this issue, we propose an adaptation of the matched accumulation concept for diffusion dispersity measurements.[65] In this method, the number of scans is adapted for each gradient strength to maintain a constant SNR across the measurement. We analyzed the dispersity of the post-reaction samples using this combined approach of a gamma-model distribution and dispersity-matched accumu-

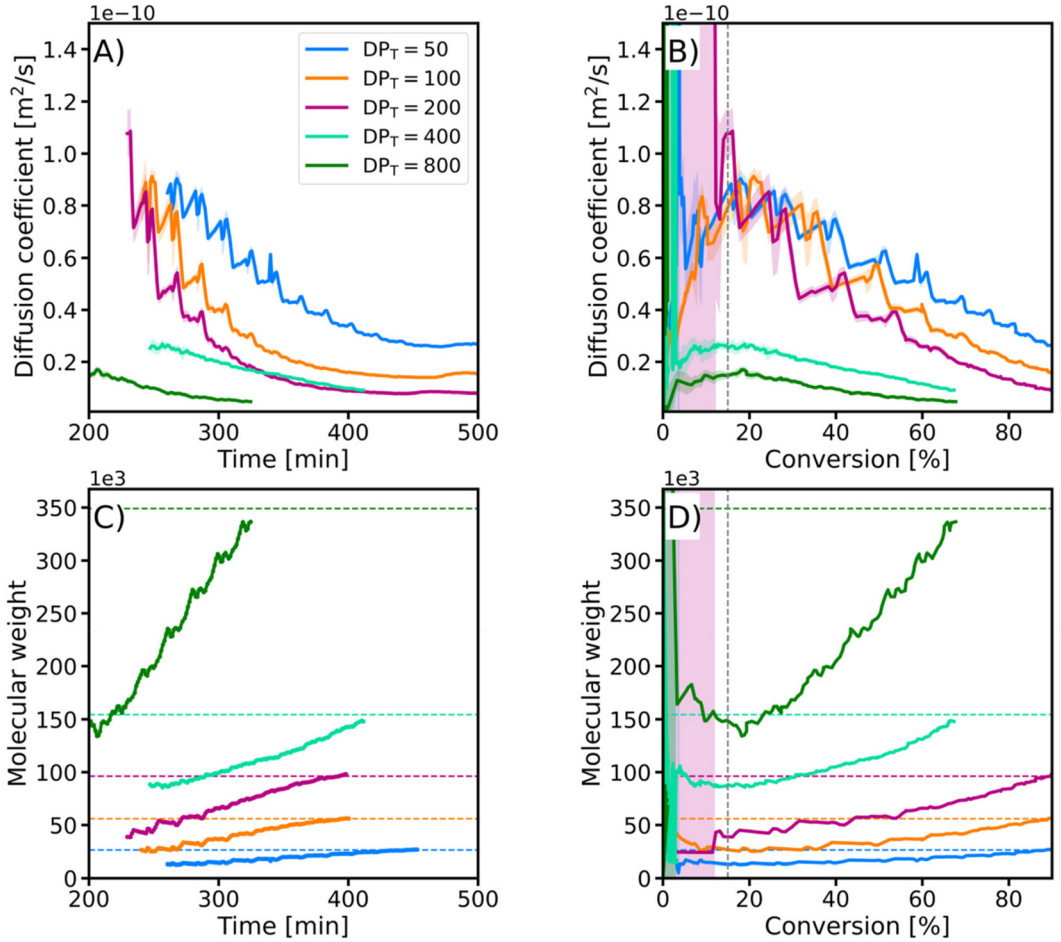

Fig. 3 Real-time monitoring of photo-ATRP for different DP_T. Evolution of the polymer's diffusion coefficient as a function of (A) time and (B) monomer conversion. Evolution of the weight-average molecular weight (M_w) as a function of (C) time and (D) monomer conversion. The vertical dotted line divides the low monomer conversion region (conv. <15%), where the diffusion coefficient estimation is prone to significant error, with the rest of the reaction. The regular small fluctuations of the diffusion coefficients and, therefore, the molecular weight, were caused by the repetitive sampling of pulsed field gradients. The shades represent the fitting error.

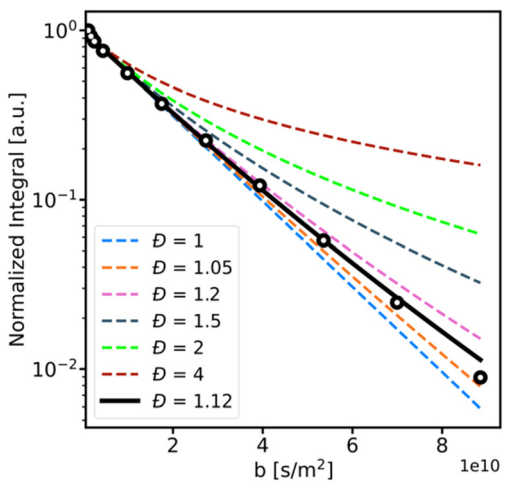

Fig. 4 The experimental data points for the diffusion decay of a polymer (DP_T = 400), as determined by a dispersity NMR measurement. The dotted lines show the theoretical decays for different dispersities, while the solid black line represents the fitted Gamma function, corresponding to a $Đ$ of 1.12.

lation. The resulting values were compared to those determined by SEC analysis (see Table 1) and showed excellent agreement.

Conclusions

In conclusion, we demonstrated the efficacy of the Time-Resolved Diffusion NMR method for monitoring the photo-ATRP in real time. Our approach allowed us to track the evolution of the diffusion coefficient and molecular weight of the polymer as the reaction proceeded under illumination. To facilitate wider adoption of this method, we developed a user-friendly program that automated reaction monitoring and enabled the polymerization to be halted at a precise monomer conversion. Finally, we showed that the Diffusion NMR, when combined with a gamma-model and dispersity-matched accumulation, is a powerful alternative to conventional size exclusion chromatography (SEC) measurements, allowing the study of the

process *in situ* with significantly less effort from the operator. Additionally, the method might be combined with a benchtop NMR spectrometer and flow setup to monitor the process inside the full-scale reactor for larger-scale polymerization.

Author contributions

M. C.: methodology, software, formal analysis, investigation, visualization, writing – original draft. M. C. C.: investigation, formal analysis, writing – original draft, writing – review and editing. F. F. W.: software. F. A. C.: investigation. K. K.: investigation, formal analysis. K. M.: writing – review and editing. G. S.: conceptualization, methodology, resources, writing – original draft, writing – review and editing, supervision, project administration, funding acquisition. M. U.: conceptualization, methodology, resources, writing – original draft, writing – review and editing, supervision, project administration, funding acquisition.

Conflicts of interest

There are no conflicts to declare.

Data availability

The NMR raw data and processing scripts used for the results shown in this manuscript are available in RepOD ICM repository at: https://doi.org/10.18150/RB78J7. The acquisition and live monitoring programs are available on GitHub at: https://github.com/murbanczyk/PhotopolymerizationMonitor.

Supplementary information (SI) is available. See DOI: https://doi.org/10.1039/d6py00103c.

Acknowledgements

M. U. and M. C would like to thank the National Science Centre, Poland, for its support in the form of an OPUS Grant (2021/41/B/ST4/01286). M. C. C and G. S acknowledge support from the Polish National Agency for Academic Exchange under the Polish Returns program (BPN/PPO/2022/1/00027) and the Polish National Science Center (2023/02/1/ST4/00009). K. K. and K. M. acknowledge support from NSF (CHE 2401112).

References

1 N. Corrigan, K. Jung, G. Moad, C. J. Hawker, K. Matyjaszewski and C. Boyer, *Prog. Polym. Sci.*, 2020, **111**, 101311.
2 K. Parkatzidis, H. S. Wang, N. P. Truong and A. Anastasaki, *Chem*, 2020, **6**, 1575–1588.
3 J. S. Wang and K. Matyjaszewski, *J. Am. Chem. Soc.*, 1995, **117**, 5614–5615.
4 S. Harrisson, R. Whitfield, A. Anastasaki and K. Matyjaszewski, *Nat. Rev. Methods Primers*, 2025, **5**, 1–20.
5 X. Pan, M. A. Tasdelen, J. Laun, T. Junkers, Y. Yagci and K. Matyjaszewski, *Prog. Polym. Sci.*, 2016, **62**, 73–125.
6 S. Dadashi-Silab, I. H. Lee, A. Anastasaki, F. Lorandi, B. Narupai, N. D. Dolinski, M. L. Allegrezza, M. Fantin, D. Konkolewicz, C. J. Hawker and K. Matyjaszewski, *Macromolecules*, 2020, **53**, 5280–5288.
7 S. Dworakowska, F. Lorandi, A. Gorczyński and K. Matyjaszewski, *Adv. Sci.*, 2022, **9**, 2106076.
8 X. Pan, N. Malhotra, A. Simakova, Z. Wang, D. Konkolewicz and K. Matyjaszewski, *J. Am. Chem. Soc.*, 2015, **137**, 15430–15433.
9 R. A. Olson, A. B. Korpusik and B. S. Sumerlin, *Chem. Sci.*, 2020, **11**, 5142–5156.
10 F. Lorandi, M. Fantin, H. Jafari, A. Gorczyński, G. Szczepaniak, S. Dadashi-Silab, A. A. Isse and K. Matyjaszewski, *J. Am. Chem. Soc.*, 2023, **145**, 21587–21599.
11 G. Szczepaniak, L. Fu, H. Jafari, K. Kapil and K. Matyjaszewski, *Acc. Chem. Res.*, 2021, **54**, 1779–1790.
12 M. A. Beres, C. Boyer, M. Hartlieb, D. Konkolewicz, G. G. Qiao, B. S. Sumerlin and S. Perrier, *ACS Polym. Au*, 2025, **5**, 184–213.
13 T. D. Svejstrup, A. Chatterjee, D. Schekin, T. Wagner, J. Zach, M. J. Johansson, G. Bergonzini and B. König, *ChemPhotoChem*, 2021, **5**, 808–814.
14 O. Tooley, W. Pointer, R. Radmall, M. Hall, T. Swift, J. Town, C. Aydogan, T. Junkers, P. Wilson, D. Lester and D. Haddleton, *ACS Polym. Au*, 2024, **4**, 311–319.
15 J. J. Haven and T. Junkers, *Eur. J. Org. Chem.*, 2017, **2017**, 6474–6482.
16 J. J. Haven, J. Vandenbergh and T. Junkers, *Chem. Commun.*, 2015, **51**, 4611–4614.
17 J. E. Puskas, P. Chan, K. B. McAuley, G. Kaszas and S. Shaikh, *Macromol. Symp.*, 2006, **240**, 18–22.
18 R. Hoogenboom, M. W. M. Fijten, C. H. Abeln and U. S. Schubert, *Macromol. Rapid Commun.*, 2004, **25**, 237–242.
19 M. Rubens, J. Van Herck and T. Junkers, *ACS Macro Lett.*, 2019, **8**, 1437–1441.
20 X. L. Wang, W. Liu, Y. Y. Yu, Y. Song, W. Q. Fang, D. Wei, X. Q. Gong, Y. F. Yao and H. G. Yang, *Nat. Commun.*, 2016, **7**, 1–7.
21 D. A. Foley, E. Bez, A. Codina, K. L. Colson, M. Fey, R. Krull, D. Piroli, M. T. Zell and B. L. Marquez, *Anal. Chem.*, 2014, **86**, 12008–12013.
22 R. Dass, W. Koźmiński and K. Kazimierczuk, *Anal. Chem.*, 2015, **87**, 1337–1343.
23 C. Jacquemmoz, F. Giraud and J.-N. Dumez, *Analyst*, 2020, **145**, 478–485.
24 B. Gouilleux, B. Charrier, E. Danieli, J. N. Dumez, S. Akoka, F. X. Felpin, M. Rodriguez-Zubiri and P. Giraudeau, *Analyst*, 2015, **140**, 7854–7858.
25 M. Urbańczyk, A. Shchukina, D. Gołowicz and K. Kazimierczuk, *Magn. Reson. Chem.*, 2019, **57**, 4–12.

26 D. Gołowicz, K. Kazimierczuk, M. Urbańczyk and T. Ratajczyk, *ChemistryOpen*, 2019, **8**, 196–200.
27 K. Kristinaityte, A. Mames, M. Pietrzak, F. F. Westermair, W. Silva, R. M. Gschwind, T. Ratajczyk and M. Urbańczyk, *J. Am. Chem. Soc.*, 2022, **144**, 13938–13945.
28 V. V. Telkki, M. Urbańczyk and V. Zhivonitko, *Prog. Nucl. Magn. Reson. Spectrosc.*, 2021, **126–127**, 101–120.
29 L. L. Jessen, K. R. Hansen, G. B. Crull, T. L. Grover and C. A. Guymon, *ACS Macro Lett.*, 2025, **14**, 847–852.
30 G. Szczepaniak, J. Jeong, K. Kapil, S. Dadashi-Silab, S. S. Yerneni, P. Ratajczyk, S. Lathwal, D. J. Schild, S. R. Das and K. Matyjaszewski, *Chem. Sci.*, 2022, **13**, 11540–11550.
31 A. Lasorsa, P. van der Meulen, E. Naumann, M. M. Lerch, R. M. Garcia, X. Lan, K. Loos, B. L. Feringa, W. Szymanski and P. C. A. van der Wel, *J. Mater. Chem. A*, 2025, **13**, 36318–36329.
32 S. Ahola and V.-V. Telkki, *ChemPhysChem*, 2014, **15**, 1687–1692.
33 O. Tooley, W. Pointer, R. Radmall, M. Hall, V. Beyer, K. Stakem, T. Swift, J. Town, T. Junkers, P. Wilson, D. Lester and D. Haddleton, *Macromol. Rapid Commun.*, 2024, **45**, 2300692.
34 L. Guduff, I. Kuprov, C. Van Heijenoort and J. N. Dumez, *Chem. Commun.*, 2017, **53**, 701–704.
35 G. Hamdoun, L. Guduff, C. Van Heijenoort, C. Bour, V. Gandon and J. N. Dumez, *Analyst*, 2018, **143**, 3458–3464.
36 M. Mayzel, J. Rosenlöw, L. Isaksson and V. Y. Orekhov, *J. Biomol. NMR*, 2014, **58**, 129–139.
37 M. Urbańczyk, D. Bernin, A. Czuroń and K. Kazimierczuk, *Analyst*, 2016, **141**, 1745–1752.
38 T. S. C. MacDonald, W. S. Price and J. E. Beves, *ChemPhysChem*, 2019, **20**, 926–930.
39 M. Urbańczyk, Y. Kharbanda, O. Mankinen and V.-V. Telkki, *Anal. Chem.*, 2020, **92**, 9948–9955.
40 L. L. Fillbrook, M. D. Nothling, M. H. Stenzel, W. S. Price and J. E. Beves, *ACS Macro Lett.*, 2022, **11**, 166–172.
41 J. E. Bramham and A. P. Golovanov, *Commun. Chem.*, 2022, **5**, 1–10.
42 P. Nitschke, N. Lokesh and R. M. Gschwind, *Prog. Nucl. Magn. Reson. Spectrosc.*, 2019, **114–115**, 86–134.
43 A. Seegerer, P. Nitschke and R. M. Gschwind, *Angew. Chem., Int. Ed.*, 2018, **57**, 7493–7497.
44 Y. Ji, D. A. DiRocco, J. Kind, C. M. Thiele, R. M. Gschwind and M. Reibarkh, *ChemPhotoChem*, 2019, **3**, 984–992.
45 C. Feldmeier, H. Bartling, E. Riedle and R. M. Gschwind, *J. Magn. Reson.*, 2013, **232**, 39–44.
46 J. Sobieski, A. Gorczyński, A. M. Jazani, G. Yilmaz and K. Matyjaszewski, *Angew. Chem., Int. Ed.*, 2025, **64**, e202415785.
47 R. Bernat, G. Szczepaniak, K. Kamiński, M. Paluch, K. Matyjaszewski and P. Maksym, *Chem. Commun.*, 2024, **60**, 843–846.
48 K. Kapil, G. Szczepaniak, M. R. Martinez, H. Murata, A. M. Jazani, J. Jeong, S. R. Das and K. Matyjaszewski, *Angew. Chem., Int. Ed.*, 2023, **62**, e202217658.
49 J. Jeong, G. Szczepaniak, S. R. Das and K. Matyjaszewski, *Chem*, 2023, **9**, 3319–3334.
50 F. Lorandi, M. Fantin and K. Matyjaszewski, *J. Am. Chem. Soc.*, 2022, **144**, 15413–15430.
51 K. Matyjaszewski, *Macromolecules*, 2012, **45**, 4015–4039.
52 D. Gołowicz, P. Kasprzak, V. Orekhov and K. Kazimierczuk, *Prog. Nucl. Magn. Reson. Spectrosc.*, 2020, **116**, 40–55.
53 A. Shchukina, M. Urbańczyk, P. Kasprzak and K. Kazimierczuk, *Concepts Magn. Reson., Part A: Bridging Educ. Res.*, 2017, **46**, e21429.
54 M. Oikonomou, J. Asencio-Hernández, A. H. Velders and M.-A. Delsuc, *J. Magn. Reson.*, 2015, **258**, 12–16.
55 K. Kazimierczuk and V. Y. Orekhov, *Angew. Chem., Int. Ed.*, 2011, **50**, 5556–5559.
56 M. Urbańczyk, D. Bernin, W. Koźmiński and K. Kazimierczuk, *Anal. Chem.*, 2013, **85**, 1828–1833.
57 W. Li, H. Chung, C. Daeffler, J. A. Johnson and R. H. Grubbs, *Macromolecules*, 2012, **45**, 9595–9603.
58 B. Grabe and W. Hiller, *Macromolecules*, 2022, **55**, 8014–8020.
59 W. Hiller, B. Grabe and J. Schonert, *Anal. Chem.*, 2024, **96**, 14902–14908.
60 F. M. Arrabal-Campos, P. Oña-Burgos and I. Fernández, *Polym. Chem.*, 2016, **7**, 4326–4329.
61 P. J. Voorter, A. McKay, J. Dai, O. Paravagna, N. R. Cameron and T. Junkers, *Angew. Chem., Int. Ed.*, 2022, **61**, e202114536.
62 M. Röding, D. Bernin, J. Jonasson, A. Särkkä, D. Topgaard, M. Rudemo and M. Nydén, *J. Magn. Reson.*, 2012, **222**, 105–111.
63 P. Mocny, T. C. Lin, R. Parekh, Y. Zhao, M. Czarnota, M. Urbańczyk, C. Majidi and K. Matyjaszewski, *ACS Appl. Mater. Interfaces*, 2024, **16**, 23932–23947.
64 E. O. Stejskal and J. E. Tanner, *J. Chem. Phys.*, 1965, **42**, 288.
65 A. Kumar, S. C. Brown, M. E. Donlan, B. U. Meier and P. W. Jeffs, *J. Magn. Reson.*, 1991, **95**, 1–9.